

**\*\*TITLE\*\***

*ASP Conference Series, Vol. \*\*VOLUME\*\*, \*\*PUBLICATION YEAR\*\**

**\*\*EDITORS\*\***

## Numerical Convergence of Hydrodynamical SPH Simulations of Cooling Clusters

Riccardo Valdarnini

*SISSA Via Beirut 2-4 34014, Trieste, Italy*

**Abstract.** The results from hydrodynamical TREESPH simulations of galaxy clusters are used to investigate the dependence of the final cluster X-ray properties upon the numerical resolution and the assumed star formation models for the cooled gas. When cold gas particles are allowed to convert into stars the final gas profiles show a well defined core radius and the temperature profiles are nearly flat. A comparison between runs with different star formation methods shows that the results of simulations, based on star formation methods in which gas conversion into stars is controlled by an efficiency parameter  $c_*$ , are sensitive to the simulation numerical resolution. In this respect star formation methods based instead on a local density threshold, as in Navarro & White (1993), are shown to give more stable results. Final X-ray luminosities are found to be numerically stable, with uncertainties of a factor  $\sim 2$ .

### 1. Introduction

Galaxy clusters are the largest virialized structures known in the universe and also bright X-ray sources. Useful cosmological information can be obtained from the statistical properties of the ensemble of X-ray clusters. X-ray observations of cluster number counts, the X-ray temperature function (Henry & Arnoud 1991; Edge et al. 1990; Henry 1997) and the X-ray luminosity function (Rosati et al. 1998; Ebeling et al. 1998) are powerful probes to constrain the values of the cosmological parameters  $\Omega_0$  and  $\sigma_8$  (Henry & Arnoud 1991; White, Efstathiou, & Frenk 1993; Bahcall & Fan 1998; Eke, Cole, & Frenk 1996; Kitayama, Sasaki, & Suto 1998)

Hydrodynamical simulations have been widely used to predict for different theoretical frameworks the time evolution of the gas and temperature distributions. The numerical methods used are either Eulerian (Cen & Ostriker 1994; Anninos & Norman 1996; Bryan & Norman 1998; Kang et al. 1994; Bryan et al. 1994, Cen 1997; Cen et al. 1995) with a fixed or adaptative grid, or Lagrangian (Evrard 1988; 1990; Thomas & Couchman 1992; Navarro, Frenk, & White 1995; Eke, Navarro, & Frenk 1998; Katz & White 1993; Yoshikawa, Itoh, & Suto 1998; Valdarnini, Ghizzardi, & Bonometto 1999) In these simulations the gas component is treated as a single adiabatic fluid, without taking into account the effects of radiative cooling, and the physical processes which can be modelled are merging, substructure formation, shocks and compressional heating of the gas. A comparison between different numerical simulations shows that they are

successful in reproducing the gross features of the cluster properties (Frenk et al. 1999). With increasing availability of computational power, numerical hydrodynamical simulations have been attempted to model the effects of radiative cooling on the gas in the formation and evolution of cluster galaxies (Katz & White 1993; Sugihara & Ostriker 1998; Anninos & Norman 1996; Yoshikawa, Jing, & Suto 2000; Pearce et al. 2000; Lewis et al. 2000). The numerical problems posed by the inclusion of gas cooling are challenging, mainly because the required increased spatial resolution also requires that one keeps under control two-body heating mechanisms. Previous simulations have produced some conflicting results (Yoshikawa, Jing, & Suto 2000; Pearce et al. 2000), thus the question of the minimum resolution in this kind of simulations is still to be fully settled.

In this contribution I will show the preliminary results that have been obtained from a series of hydrodynamical SPH simulations of galaxy clusters. The simulations have different numerical resolution and include the effects on the gas component of radiative losses, star formation and energy feedback from SN. Final profiles are compared in order to assess the effects of numerical resolution, or different star formation prescriptions, on the cluster X-ray variables.

## 2. Simulations

In a previous paper (Valdarnini et al. 1999, hereafter VGB) a large set of hydrodynamical simulations was used to study the global X-ray cluster morphology and its evolution. The simulations were run using a TREESPH code with no gas cooling or heating. In order to assess the numerical reliability of the numerical integrations, four different clusters were selected as a representative sample of all the simulation clusters. For this cluster sample a large set of different integrations was performed by varying two numerical input parameters: the number of particles and the softening parameters. I refer to VGB for a detailed description of the simulations. In Valdarnini (2001) I have used the same cluster sample to study the effects of including in the simulations additional physics such as gas cooling and star formation. I will report here the results for the cluster with label  $\Lambda$ CDM00 in VGB. This is the most massive cluster ( $M_v \simeq 1.5 \cdot 10^{15} M_\odot$ ) extracted from a cosmological  $\Lambda$ CDM N-body simulation with size  $L = 200h^{-1} Mpc$ , matter density  $\Omega_m = 0.3$  and Hubble constant  $H_0 = 70 Km \ sec^{-1} \ Mpc^{-1}$ . In order to check the effects of radiative cooling for this cluster a set of TREESPH simulations was performed, with initial conditions provided by the cosmological simulation, and different values of the gas softening parameter  $\varepsilon_g$  and number of gas particles  $N_g$ . For this cluster Table 1 reports the values of  $\varepsilon_g$  and  $N_g$  for the simulation runs. The generic simulation has cluster index cl00 -  $j$ , with  $j = 00, 01, \dots, 05$ . The cluster cl00 - 00 is the reference case without cooling. The effects of radiative cooling are modelled in these simulations by adding to the SPH thermal energy equation an energy-sink term. The total cooling function includes contribution from recombination and collisional excitation, bremsstrahlung and inverse Compton cooling.

Allowing the gas to cool radiatively will produce dense clumps of gas at low temperatures ( $\simeq 10^4 \text{ }^\circ K$ ). In these regions the gas will be thermally unstable and will likely meet the physical conditions to form stars. In TREESPH simulations

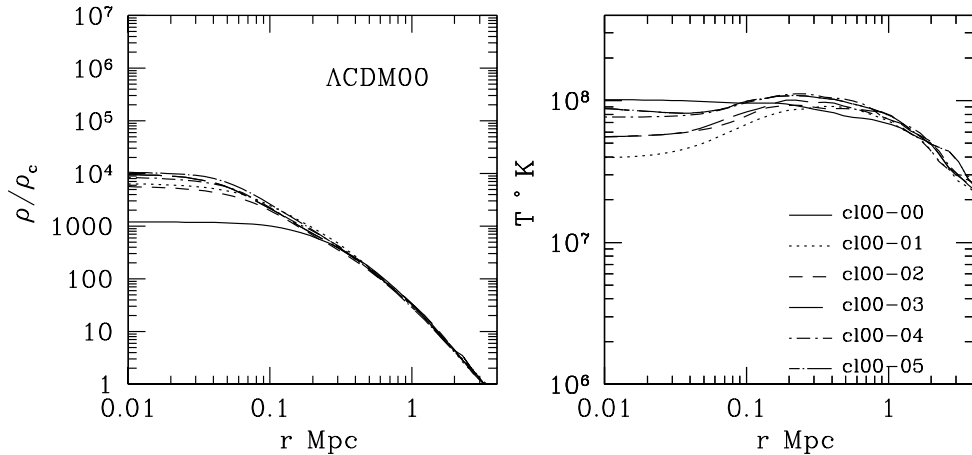


Figure 1. Final density and temperature profiles in the simulation runs including radiative cooling and star formation. Density is in units of the critical density. Different curves are for integrations with different numbers of particles and different softening parameters (see Table 1). The simulation run with index  $-00$  is the integration without cooling.

star formation (SF) processes have been implemented using different approaches. According to Katz, Weinberg, & Hernquist (1996, hereafter KWH) a gas particle is in a star forming region if the flow is convergent and the local sound crossing time is larger than the dynamical time (i.e. the fluid is Jeans unstable). In a simplified version Navarro & White (1993, hereafter NW) assume as a sufficient condition that a gas particle must be in a convergent flow and its density exceeds a threshold ( $\rho_g > \rho_{g,c} = 7 \cdot 10^{-26} \text{ g cm}^{-3}$ ).

If a gas particle meets these criteria then it is selected as an eligible particle to form stars. The local star formation rate (SFR) obeys the equation

$$d\rho_g/dt = -c_\star \rho_g / \tau_g = -d\rho_\star / dt, \quad (1)$$

where  $\rho_g$  is the gas density,  $\rho_\star$  is the star density,  $c_\star$  is a characteristic dimensionless efficiency parameter,  $\tau_g$  is the local collapse time and it is the maximum of the local cooling time  $\tau_c$  and the dynamical time  $\tau_d$ . Gas particles with  $T \lesssim 10^4 \text{ K}$  have long cooling times and  $\tau_g = \tau_d$ . At each step the probability that a gas particle will form stars in a time step  $\Delta t$  is compared with a uniform random number. If the test is successful then a mass fraction  $\varepsilon_\star$  of the gas mass is converted into a new collisionless particle. This star particle has the position, velocity and gravitational softening of the original gas particle. Typical assumed values are  $\varepsilon_\star = 1/3$  and  $c_\star = 0.1$  (KWH). For the local SFR, NW adopt Eq. 1 with  $c_\star = 1$ ,  $\tau_g = \tau_d$  and  $\varepsilon_\star = 1/2$  when a gas particle can convert part of its mass into a star particle.

The numerical tests have been performed following the NW prescriptions for selecting gas particles which can form stars. Once a star particle is created it can release energy into the surrounding gas through supernova (SN) explosions. All the stars with mass above  $8M_{\odot}$  end as a SN, leaving a  $1.4M_{\odot}$  remnant. The SN energy ( $\simeq 10^{51} \text{erg}$ ) is released gradually into the gas according to the lifetime of stars of different masses.

### 3. Results

The final radial gas density and temperature profiles are shown in Fig. 1. As can be inferred from Table 1, the numerical strategy has been to perform runs of increasing spatial resolution in order to resolve the core radius of the gas density profile. The most important result is that the inclusion of a star formation prescription has been effective in removing the cold gas particles ( $T \lesssim 10^4 \text{K}$ ) from the cluster center. In all the simulations the gas density profiles have a well-defined core radius, with size  $r_c \simeq 50 - 100 \text{Kpc}$ , approximately 0.05 of the virial radius  $r_v$  ( $\simeq 2.9 \text{Mpc}$ ). The shapes of the temperature profiles show that convergence is achieved for  $N_g \gtrsim 20,000$ . All the central values for the gas temperatures at  $r = 10 \text{Kpc}$  are within a factor  $\simeq 1.5$  for the highest resolution simulation runs. The profiles increase inwards from the virial radius up to  $\simeq 100 - 200 \text{Kpc}$ . Thereafter the profiles stay almost flat, or with a modest decline in  $T(r)$  towards  $r = 0$ . There is not a strong drop of the temperature in the very central region. Final X-ray luminosities are quite stable ( $L_X \simeq 2 \cdot 10^{45} \text{ergsec}^{-1}$ ) versus the simulation numerical resolution. Compared to the non-radiative run the luminosities increase by a factor  $\simeq 2$ .

A different question is the sensitivity of the estimated cluster properties to the numerical method used to describe star formation in the hydrodynamical simulations. To this end three simulations were performed with the same numerical parameters as for the cl00 – 05 run, but using different SF methods or parameters. The NW simulation (I) is the standard case showed in Fig. 1. In the other two runs (II and III) the KWH prescription is adopted for converting gas particles into stars, but with different values of the star formation efficiency parameter  $c_{\star}$ : 0.1 and 1. (see Fig. 2). The most important differences are found between the KWH simulations with different  $c_{\star}$ . The differences are dramatic in the final X-ray luminosities, which differ by a factor  $\simeq 40$ . The source of this discrepancy relies in the different gas density profiles, which have substantial differences in the cluster core regions for  $r \lesssim 100 \text{Kpc}$ . These differences are localized at the cluster center, beyond  $r \simeq 100 \text{Kpc}$  all the profiles converge, as it is shown in the plots of Fig. 2. The temperature profiles have a peak value of  $\simeq 10^8 \text{K}$  at  $r \simeq 100 \text{Kpc}$  and thereafter decline outward by a factor  $\sim 2$  out to  $r_v$ . Below  $\sim 100 \text{Kpc}$  the profiles instead show large differences. Compared to the NW run the simulation with  $c_{\star} = 0.1$  has gas temperatures which decline inwards by a factor  $\sim 10$  from  $\sim 100 \text{Kpc}$  down to  $r \sim 10 \text{Kpc}$ . These radial decays follow because of the less efficient conversion of the cooled gas into stars compared to the NW run. There is a remarkable agreement for the ratio of cluster mass locked into stars to the gas mass, which is  $\simeq 10\%$  at  $r_v$  for all the runs considered. In order to assess the effects of numerical resolution upon final results simulations I, II and III have been run again but with a number

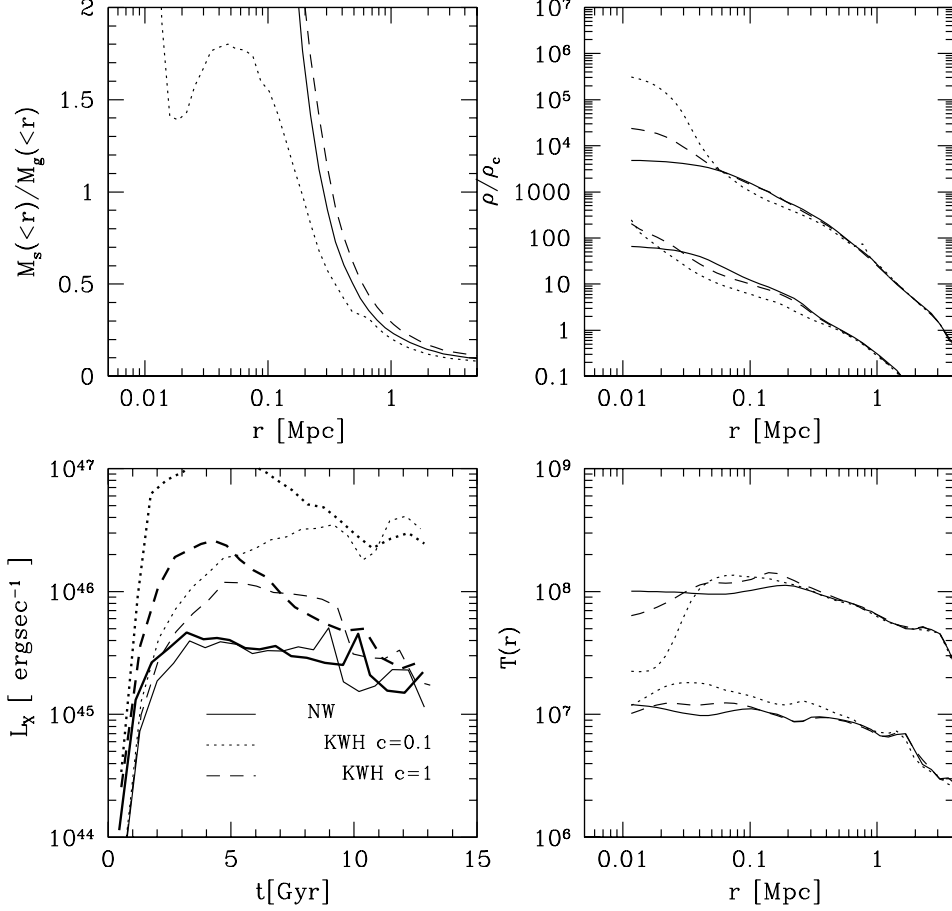


Figure 2. Plots showing several cluster properties in simulation runs with different SF prescriptions. The simulation parameters are those of cl00 – 05 (see Table 1). The continuous line refers to the NW method, the others to KWH with different  $c_*$  ( $c$  in the bottom left panel). *Top left:* ratio of the star mass within the radius  $r$  over the gas mass within  $r$ . *Top right:* final radial density behavior for the gas component. The simulation results are compared with the corresponding high-resolution runs (H). The H simulations have the same SF parameters of the parent simulations, but the numerical parameters are given in the last row of Table 1. To facilitate a comparison the radial profiles of the high resolution results have been shifted downward by  $10^k$ ,  $k = 2$  for densities and  $k = 1$  for temperatures. *Bottom right:* Radial temperature profiles. *Bottom left :* X-ray luminosity versus time, the thick lines correspond to the high resolution simulations.

of particles increased by a factor  $\simeq 3$  (cl00 – 05H). These simulations will be referred as IH, IIH and IIIH, respectively. The simulation results are shown in Fig. 2. For simulations IH there are not appreciable differences in the radial profiles. This confirms the previous results, that is the NW runs have reached numerical convergence in the physical variables for the numerical parameters of the cl00 – 05 simulation of Table 1. The profiles of simulation IIH are instead different from those of run II at  $r \lesssim 50 Kpc$ . The strong drop in  $T(r)$  has been removed and the gas density profile is much closer to the NW one. Simulation IIIH yields final profiles very similar to the ones of the parent simulation. The bottom left panel of Fig. 2 shows that high resolution runs have final X-ray luminosities which can differ within a factor  $\sim 2$  from the parent simulations.

To summarize, the above results demonstrate that simulations I and III have an adequate numerical resolution to reliably predict X-ray cluster properties, such as the X-ray luminosity. For simulation II ( KWH with  $c_\star = 0.1$  ) there are large differences at the cluster core between the final profiles when the numerical resolution is increased. For the simulation runs I and III  $L_X \simeq 10^{45} ergsec^{-1}$ , while  $L_X \simeq 4 \cdot 10^{46} ergsec^{-1}$  for the run with  $c_\star = 0.1$ . Thus simulations I and III are consistent at the  $1\sigma$  level with the  $L_{bX} - T_X$  relation derived from a sample of cooling flow clusters (Allen & Fabian 1998). For simulation II the predicted cluster temperature is outside the  $2\sigma$  limits.

$\Lambda$ CDM00	$\varepsilon_g^a$	$m_g^b$	$m_d^c$	$N_g^d$	$N_d^e$	$N_T^f$	$\theta^g$	$z_{in}^h$
cl00-00	56	$3.01 \cdot 10^{10}$	$2.64 \cdot 10^{11}$	5503	6295	16463	0.7	10.
cl00-01	56	$3.01 \cdot 10^{10}$	$2.64 \cdot 10^{11}$	5503	6295	16463	0.7	10.
cl00-02	28	$3.01 \cdot 10^{10}$	$2.64 \cdot 10^{11}$	5503	6295	16463	0.7	10.
cl00-03	21	$1.45 \cdot 10^{10}$	$1.28 \cdot 10^{11}$	11480	14208	35408	0.7	10.
cl00-04	15.4	$1.45 \cdot 10^{10}$	$1.28 \cdot 10^{11}$	11480	14208	35408	0.7	10.
cl00-05	21	$7.47 \cdot 10^9$	$6.57 \cdot 10^{10}$	22575	25391	67388	0.7	19.
cl00-05H	10.5	$2.45 \cdot 10^9$	$2.12 \cdot 10^{10}$	69599	74983	204799	1.0	29.

Table 1. Simulation parameters of the test runs for the  $\Lambda$ CDM00 cluster. cl00 – 00 is the reference case with no cooling, taken from VGB. <sup>a</sup>: gravitational softening parameter for the gas in  $h^{-1}$  Kpc. <sup>b</sup>: mass of the gas particles in  $h^{-1} M_\odot$  (the cosmology is for  $\Omega_m = 0.3$  and  $h = 0.7$ ). <sup>c</sup>: mass of the dark particles. <sup>d</sup>: number of gas particles. <sup>e</sup>: as in the previous column but for dark particles. <sup>f</sup>: total number of simulation particles. <sup>g</sup>: value of the treecode gravitational tolerance parameter. <sup>h</sup>: initial redshift for the simulation. The last row gives the numerical parameters for the high-resolution runs used to test different SF methods. For these runs gravitational quadrupole corrections were enabled.

**References**

- Allen, S.W., & Fabian, A.C. 1998, MNRAS, 297, L57
- Anninos, P., & Norman, M.L. 1996, ApJ, 459, 12
- Bahcall, N.A., & Fan, X. 1998, ApJ, 504, 1
- Bryan, G.L., Cen, R., Norman, M.L., Ostriker, J.P., & Stone, J.M. 1994, ApJ, 428, 405
- Bryan, G.R., & Norman, M.L. 1998, ApJ, 495, 80
- Cen, R. 1997, ApJ, 485, 39
- Cen R., & Ostriker J., 1994, ApJ, 429, 4
- Cen, R., Kang, H., Ostriker, J.P., & Ryu, D. 1995, ApJ 451, 436
- Ebeling, H. et al. 1998, MNRAS, 301, 881
- Edge, A.C., Stewart, G.C., Fabian, A.C., & Arnaud, K.A. 1990, MNRAS, 245, 559
- Eke, V.R., Cole, S., & Frenk, C.S. 1996, MNRAS, 282, 263
- Eke, V.R., Navarro, J.F., & Frenk, C.S. 1998, ApJ, 503, 569
- Evrard, A.E. 1988, MNRAS, 235, 911
- Evrard, A.E. 1990, ApJ, 363, 349
- Frenk, C.S. et al. 1999, ApJ, 525, 554
- Henry, J.P., & Arnaud, K.A. 1991, ApJ, 372, 410
- Henry, J.P. 1997, ApJ, 489, L1
- Kang, H. , Cen, R. , Ostriker, J.P., & Ryu, D. 1994, ApJ, 428, 1
- Katz, N., & White, S.D.M. 1993, ApJ, 412, 455
- Katz, N., Weinberg, D.H., & Hernquist, L. 1996, ApJS, 105, 19
- Kitayama, T., Sasaki, S., & Suto, Y. 1998, PASJ, 50, 1
- Lewis, G.F., Babul, A., Katz, N., Quinn, T., Hernquist, L., & Weinberg, D.H. 2000, ApJ 536, 623
- Navarro, J., & White, S.D.M. 1993, MNRAS, 265, 271 (NW)
- Navarro, J., Frenk C.S., & White, S.D.M. 1995, MNRAS, 275, 720
- Pearce, F.R., Thomas, P.A., Couchman, H.M.P., & Edge, A.C. 2000, MNRAS 317, 1029
- Rosati, P., Della Ceca, R., Norman, C., & Giacconi, R. 1998, ApJ, 492, L21
- Sugimotohara, T., & Ostriker, J.P. 1998, ApJ, 507, 16
- Thomas, P.A., & Couchman, H.M.P. 1992, MNRAS, 257, 11
- Valdarnini, R., Ghizzardi, S., & Bonometto, S. 1999, New Astr, 4, 71 (VGB)
- Valdarnini, R. 2001, in preparation
- White, S.D.M., Efstathiou, G., & Frenk, C.S. 1993, MNRAS, 262, 1023
- Yoshikawa, K., Itoh, M., & Suto, Y. 1998, PASJ, 50, 203
- Yoshikawa, K., Jing, Y.P., & Suto, Y. 2000, ApJ, 535, 593 (YJS)